CHEMISTRY OF MATERIALS

Article

pubs.acs.org/cm

Mechanism of Thermal Al_2O_3 Atomic Layer Etching Using Sequential Reactions with $Sn(acac)_2$ and HF

Younghee Lee,[†] Jaime W. DuMont,[†] and Steven M. George*[,†,‡]

[†]Department of Chemistry and Biochemistry and [‡]Department of Mechanical Engineering, University of Colorado, Boulder, Colorado 80309, United States

ABSTRACT: Thermal Al_2O_3 atomic layer etching (ALE) can be performed using sequential, self-limiting reactions with tin(II) acetylacetonate ($Sn(acac)_2$) and HF as the reactants. To understand the reaction mechanism, *in situ* quartz crystal microbalance (QCM) and Fourier transform infrared (FTIR) measurements were conducted versus temperature. The mass change per cycle (MCPC) increased with temperature from −4.1 ng/(cm^2 cycle) at 150 °C to −18.3 ng/(cm^2 cycle) at 250 °C. Arrhenius analysis of the temperature-dependent MCPC values yielded an activation barrier for Al_2O_3 ALE of E = 6.6 ± 0.4 kcal/mol. The mass changes after the individual $Sn(acac)_2$ and HF exposures also varied with temperature. The mass changes after the $Sn(acac)_2$ exposures were consistent with more $Sn(acac)_2$ surface reaction products remaining at lower temperatures. The mass changes after the HF exposures were consistent with more AlF_3 species remaining at higher temperatures. The FTIR spectroscopic analysis observed Al_2O_3 etching by measuring the loss of absorbance of Al−O stretching vibrations in the Al_2O_3 film. The infrared absorbance of the acetylacetonate vibrational features from $Sn(acac)_2$ surface reaction products was also smaller at higher temperatures. The correlation between the MCPC values and the acetylacetonate infrared absorbance suggested that the Al_2O_3 ALE rate is inversely dependent on the acetylacetonate surface coverage. In addition, the QCM and FTIR measurements explored the nucleation of the Al_2O_3 ALE. A large mass gain and loss of infrared absorbance of Al−O stretching vibrations after the initial HF exposure on the Al_2O_3 film was consistent with the conversion of Al_2O_3 to AlF_3. FTIR experiments also observed the formation of AlF_3 after the initial HF exposure and the presence of AlF_3 on the surface after each HF exposure during Al_2O_3 ALE. In the proposed reaction mechanism, AlF_3 is the key reaction intermediate during Al_2O_3 ALE. HF converts Al_2O_3 to AlF_3 prior to removal of AlF_3 by $Sn(acac)_2$.

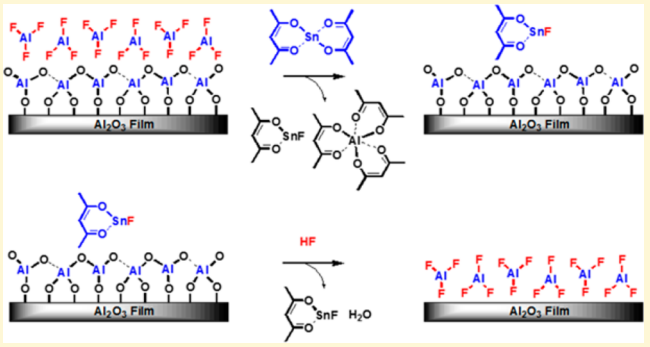

I. INTRODUCTION

Atomic layer etching (ALE) is a technique that can remove thin films with atomic layer control using sequential, self-limiting surface reactions.[1−3] ALE is the opposite of atomic layer deposition (ALD) which can provide conformal and atomic layer controlled film deposition.[4] ALD and ALE are both important techniques to provide thin film engineering at the atomic level.[5,6] ALE processes have been previously reported using ion-enhanced or energetic noble gas atom-enhanced surface reactions.[1−3] During these ALE processes, a halogen is first adsorbed on the surface of the material. Ion or noble gas atom bombardment is then used to desorb halogen compounds that etch the material. Based on this process, ALE has been reported for Si,[2,3,7−11] Ge,[6,12] and compound semiconductors.[13−16] ALE has also been demonstrated for a variety of metal oxides[17−21] and various carbon substrates.[22−24]

The ALE of Al_2O_3 was recently reported using sequential, self-limiting thermal reactions with $Sn(acac)_2$ and HF as the reactants.[25] The Al_2O_3 samples were Al_2O_3 atomic layer deposition (ALD) films grown using trimethylaluminum and H_2O. The HF source was HF−pyridine. The linear removal of Al_2O_3 was observed at temperatures from 150 to 250 °C without the use of ion or noble gas atom bombardment. An Al_2O_3 ALE etch rate of 0.27 Å/cycle was measured at 200 °C.[25] The ALE etch rates also increased at higher temperatures. The $Sn(acac)_2$ and HF thermal reactions were both self-limiting versus exposure. The Al_2O_3 films also did not roughen versus the number of Al_2O_3 ALE cycles.[25] In addition, the ALE of HfO_2 has also been recently demonstrated using $Sn(acac)_2$ and HF as the reactants.[26]

The overall Al_2O_3 etching reaction was proposed to follow the reaction: $Al_2O_3 + 6Sn(acac)_2 + 6HF \rightarrow 2Al(acac)_3 + 6SnF(acac) + 3H_2O$.[25] In the surface reactions, the $Sn(acac)_2$ reactant was suggested to donate acac to the substrate to produce $Al(acac)_3$. The HF reactant was assumed to allow SnF(acac) and H_2O to leave as reaction products.[25] An adlayer of AlF_3 was proposed to exist on the Al_2O_3 surface after HF exposures.[25] $Sn(acac)_2$ adsorption products were also believed to exist on the Al_2O_3 surface after $Sn(acac)_2$ exposures.

Received: January 23, 2015
Revised: April 17, 2015
Published: April 24, 2015

DOI: 10.1021/acs.chemmater.5b00300
Chem. Mater. 2015, 27, 3648−3657

In this study, quartz crystal microbalance (QCM) measurements determined the Al_2O_3 etch rates and the mass changes after individual $Sn(acac)_2$ and HF exposures versus temperature. The temperature dependence of the mass change per cycle (MCPC) and the individual mass changes during the $Sn(acac)_2$ and HF exposures helped to formulate a mechanism for Al_2O_3 ALE. In addition, FTIR vibrational spectroscopy analysis monitored the Al_2O_3 etching and characterized the surface species after the $Sn(acac)_2$ and HF exposures. The combination of these QCM and FTIR studies leads to the understanding of the key reaction intermediates during Al_2O_3 ALE and the reaction mechanism for thermal Al_2O_3 ALE.

II. EXPERIMENTAL SECTION

A. Viscous Flow Reactor Equipped for *in Situ* QCM Measurements. Al_2O_3 ALE was monitored using *in situ* QCM experiments in a viscous flow reactor.[27] The QCM sensor was an RC-cut quartz crystal[28] (gold coated and polished, 6 MHz, Colnatec). This QCM sensor was mounted in a bakeable sensor head (BSH-150, Inficon) and then sealed with high temperature epoxy (Epo-Tek H21D, Epoxy Technology). All of the QCM measurements were recorded by a film deposition monitor (Maxtek TM-400, Inficon). The reactor temperature was maintained by a PID temperature controller (2604, Eurotherm) at 150−250 °C during the reactions. After changing temperatures, the reactor temperature was allowed to stabilize for at least 2 h before performing new QCM measurements. The pressure in the reactor was measured using a bakeable capacitance manometer (Baratron 121A, MKS).

The reactor was pumped using a mechanical pump (Pascal 2015SD, Alcatel). A constant N_2 carrier gas flow of 150 cm^3(STP) min^{-1} was streamed through the reactor. This N_2 gas flow was supplied by three separate mass flow controllers (Type 1179A, MKS). An additional N_2 purge gas flow of 20 cm^3(STP) min^{-1} passed through the QCM housing and prevented deposition on the back side of the QCM sensor. The background pressure in the reactor resulting from the total N_2 gas flow of 170 cm^3(STP) min^{-1} was ∼1 Torr.

Al_2O_3 ALE was performed using tin(II) acetylacetonate ($Sn(acac)_2$, 37−38% Sn, Gelest) and HF−pyridine (70 wt % HF, Sigma-Aldrich) as the reactants. HF−pyridine is known as "Olah's reagent" and is a convenient reservoir for anhydrous HF.[29] The HF pressure from HF−pyridine is 90−100 Torr at room temperature.[26] $Sn(acac)_2$ and HF−pyridine were transferred to stainless steel bubblers in a dry N_2-filled glovebag. The bubbler for HF-pyridine was lined with a gold coating. The $Sn(acac)_2$ precursor was maintained at 100 °C and produced a pressure transient of 15−20 mTorr using a pneumatic valve for dosing. The HF−pyridine precursor was held at room temperature and produced a pressure transient of 80 mTorr using two pneumatic valves and one metering valve for dosing.

The Al_2O_3 films were deposited on the QCM sensor by Al_2O_3 ALD. The Al_2O_3 ALD films were grown using at least 100 cycles of Al_2O_3 ALD using TMA (97%, Sigma-Aldrich) and H_2O (deionized water, Chromasolv for HPLC, Sigma-Aldrich). The TMA and H_2O precursors were held at room temperature. The Al_2O_3 films were deposited on the QCM sensor before each ALE reaction.

B. FTIR Spectroscopy Measurements. The *in situ* FTIR studies were performed in a reactor equipped with an FTIR spectrometer that has been described previously.[30] The reactor was pumped using a mechanical pump (TRIVAC D8B, Oerlikon Leybold Vacuum). The FTIR spectrometer (Nicolet 6700 FTIR, Thermo Scientific) utilized a liquid-N_2-cooled mercury cadmium telluride (MCT-B) detector. Dry, CO_2-free air was employed to purge the spectrometer, mirror, and detector setup. Each spectrum consisted of a total of 100 scans at 4 cm^{-1} resolution from 400 to 4000 cm^{-1}.

The transmission FTIR measurements were performed on high surface area ZrO_2 nanoparticles (99.95%, US Research Nanomaterials Inc.) with an average diameter of 20 nm and high surface area SiO_2 nanoparticles (99.5%, US Research Nanomaterials Inc.) with an average diameter of 15−20 nm. The ZrO_2 nanoparticles absorb infrared radiation between ∼400 and 800 cm^{-1}. The SiO_2 nanoparticles absorb infrared radiation between 400 and 650 cm^{-1}, between 700 and 875 cm^{-1}, and between 925 and 1400 cm^{-1}. These absorption regions leave available windows to observe absorbance from the species in Al_2O_3 ALD and Al_2O_3 ALE. The high surface area of these nanoparticles was needed to enhance the signal-to-noise ratio.[31] Sample preparation involved pressing the ZrO_2 or SiO_2 nanoparticles into a tungsten grid support (Tech-Etch).[31,32] The tungsten grids had dimensions of 2 × 3 cm^2. Each grid was 50 μm thick with 100 grid lines per inch.

The tungsten grid could be resistively heated using a DC power supply (6268B, 20 V/20A, Hewlett-Packard). The voltage output of the power supply was controlled by a PID temperature controller (Love Controls 16B, Dwyer Instruments, Inc.). A type K thermocouple was fixed to the bottom of the tungsten grid with epoxy (Ceramabond 571, Aremco) that attached and electrically isolated the thermocouple.

A consistent cleaning procedure of the ZrO_2 nanoparticles/grid support was used to produce a reproducible starting surface. Prior to film deposition, the temperature of the sample support was increased to 500 °C for ∼2 min to degas and clear adventitious carbon from the ZrO_2 nanoparticles. Since this procedure also depleted the hydroxyl groups from the ZrO_2 surface, a ∼2 s H_2O dose was used to rehydroxylate the surface. This procedure consistently removed any carbon-related vibrational modes and resulted in a clean ZrO_2 starting surface with absorbances attributed only to O−H stretching vibrations and bulk ZrO_2 modes. This cleaning procedure was not utilized for the SiO_2 nanoparticles because rehydroxylation of the SiO_2 surface is very difficult after dehydroxylation.[33] The dehydroxylated siloxane surface is hydrophobic and does not easily adsorb H_2O to produce the silanol surface.[34]

The Al_2O_3 ALE reactions were performed using sequential exposures of $Sn(acac)_2$ (37−38% Sn, Gelest) and HF−pyridine (70 wt % HF, Sigma-Aldrich). Static dosing of the ALE precursors was utilized to achieve self-limiting behavior on the high surface area particle substrates. Each $Sn(acac)_2$ exposure consisted of a ∼1.0 Torr static dose for 15 s followed by a 120 s purge. Each HF−pyridine exposure consisted of a ∼1.5 Torr static dose for 15 s followed by a 120 s purge. The Al_2O_3 films were grown by Al_2O_3 ALD using TMA (97%, Sigma-Aldrich) and H_2O (Chromasolv for HPLC, Sigma-Aldrich). The HF−pyridine, TMA, and H_2O precursors were maintained at room temperature. The stainless steel bubbler containing $Sn(acac)_2$ was held at 100 °C.

For a direct comparison between the FTIR studies at different temperatures, the sample remained fixed during Al_2O_3 ALD and Al_2O_3 ALE. An Al_2O_3 film was grown using 10 cycles of Al_2O_3 ALD at 200 °C. Subsequently, 10 cycles of Al_2O_3 ALE were performed at 200 °C followed by 8 cycles of Al_2O_3 ALE at both 250 and 300 °C. The FTIR spectra monitored at 250 and 300 °C were recorded during the last two cycles of Al_2O_3 ALE.

III. RESULTS AND DISCUSSION

A. QCM Measurements versus Temperature. Figure 1 displays the mass change during 100 ALE cycles of Al_2O_3 using $Sn(acac)_2$ and HF reactions at 150, 175, 200, 225, and 250 °C. Some of these QCM results were presented earlier.[25] One ALE cycle consisted of a $Sn(acac)_2$ exposure of 1 s, an N_2 purge of 30 s, a HF exposure of 1 s, and a second N_2 purge of 30 s. This reaction sequence is represented as 1−30−1−30. The initial Al_2O_3 ALD films were grown by 100 cycles of Al_2O_3 ALD using TMA and H_2O with a sequence of 1−20−1−20.

The mass changes versus time during Al_2O_3 ALE are linear for all temperatures. The mass change per cycle (MCPC) increases with temperature from −4.1 ng/(cm^2 cycle) at 150 °C to −18.3 ng/(cm^2 cycle) at 250 °C.[25] These MCPCs correspond to etch rates that vary from 0.14 Å/cycle at 150 °C to 0.61 Å/cycle at 250 °C. The determination of these etch rates is based on the Al_2O_3 ALD film density of 3.0 g/cm^3.

DOI: 10.1021/acs.chemmater.5b00300
Chem. Mater. 2015, 27, 3648−3657

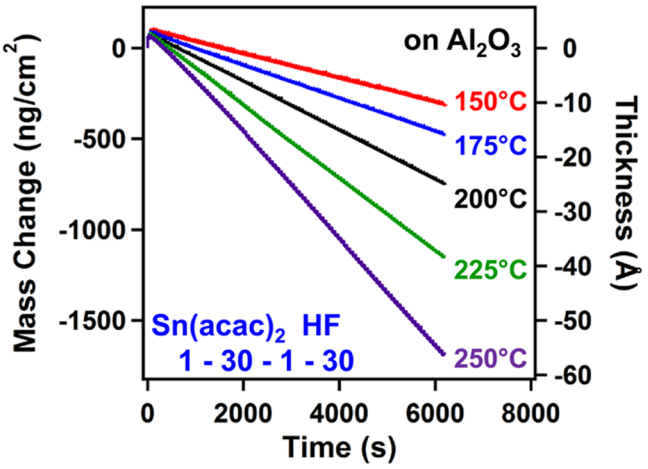

Figure 1. Mass change versus time for Al_2O_3 ALE using sequential $Sn(acac)_2$ and HF exposures at 150, 175, 200, 225, and 250 °C.

Parts a, b, and c of Figure 2 show enlargements of the mass changes during three cycles in the steady-state etching regime for Al_2O_3 ALE at 150, 200, and 250 °C, respectively, in Figure 1. Figure 2a shows a gradual mass decrease after a small mass gain during the $Sn(acac)_2$ exposure at 150 °C. A small mass gain of ΔM_{Sn} = +0.19 ng/cm^2 was observed after the $Sn(acac)_2$ exposure for 1 s at 150 °C. This behavior suggests $Sn(acac)_2$ adsorption followed by either the removal of reaction products and/or $Sn(acac)_2$ desorption. In contrast, a mass decrease of ΔM_{HF} = −4.3 ng/cm^2 was observed after the HF exposure for 1 s at 150 °C. This mass decrease is consistent with the removal of $Sn(acac)_2$ surface reaction products.

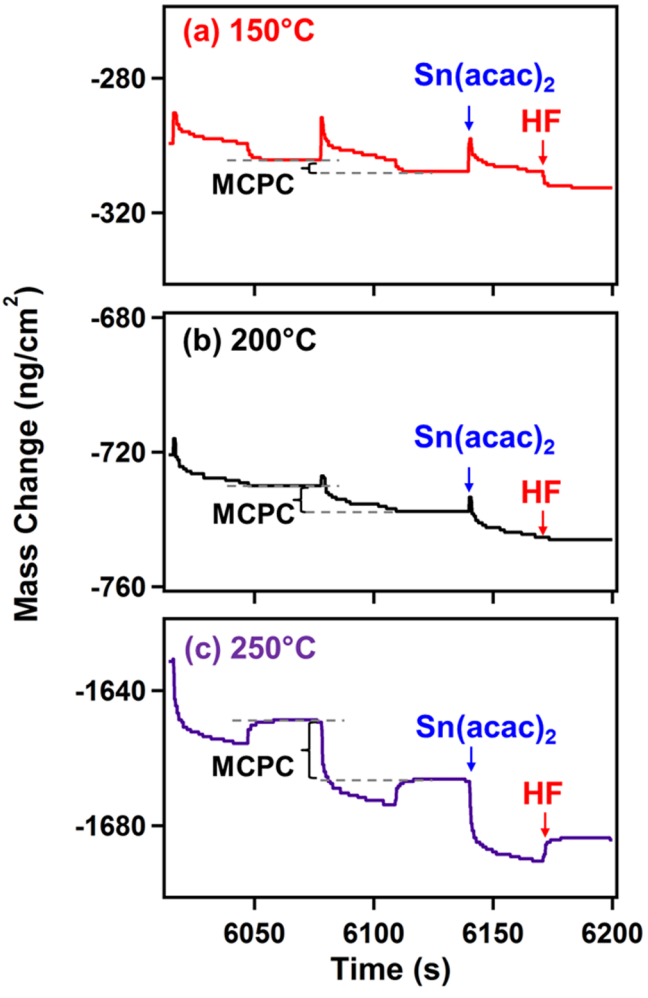

Figure 2. Expansion of linear region of Figure 1 showing the individual mass changes during the sequential $Sn(acac)_2$ and HF exposures at 150, 200, and 250 °C.

The mass changes are different at 200 °C. After a $Sn(acac)_2$ exposure for 1 s at 200 °C, Figure 2b shows a mass loss of ΔM_{Sn} = −8.1 ng/cm^2. In addition, an HF exposure for 1 s leads to a small mass loss of ΔM_{HF} = −0.28 ng/cm^2. The mass changes continue to evolve at 250 °C. Figure 2c shows a larger mass loss of ΔM_{Sn} = −24.0 ng/cm^2 after 1 s of $Sn(acac)_2$ exposure at 250 °C. In contrast, the HF exposure leads to a mass gain instead of a mass loss. A mass gain of ΔM_{HF} = +5.7 ng/cm^2 was observed after 1 s of HF exposure.

The differences between the mass changes at different temperatures can be qualitatively understood in terms of more stable $Sn(acac)_2$ surface reaction products at lower temperature and more AlF_3 formation at higher temperatures. If more surface species remain following $Sn(acac)_2$ exposures at lower temperatures, then there is a mass gain after the $Sn(acac)_2$ reaction and more surface species that can be lost during the HF reaction. Likewise, larger mass losses after the $Sn(acac)_2$ exposure and mass gains following the HF exposure at higher temperature can be qualitatively understood in terms of AlF_3 formation. More AlF_3 may form by the reaction of HF with Al_2O_3 at higher temperatures. This AlF_3 layer is then removed by the $Sn(acac)_2$ exposure and leads to a pronounced mass loss.

Figure 3 shows the MCPC and the ΔM_{Sn}/MCPC ratio during 100 cycles at 200 °C. The MCPC is defined by MCPC = ΔM_{Sn} + ΔM_{HF}. Figure 3a displays ΔM_{Sn}, ΔM_{HF}, and MCPC for the same 100 cycles of Al_2O_3 ALE reaction on the Al_2O_3 surface at 200 °C as shown in Figure 1. The MCPC reaches a

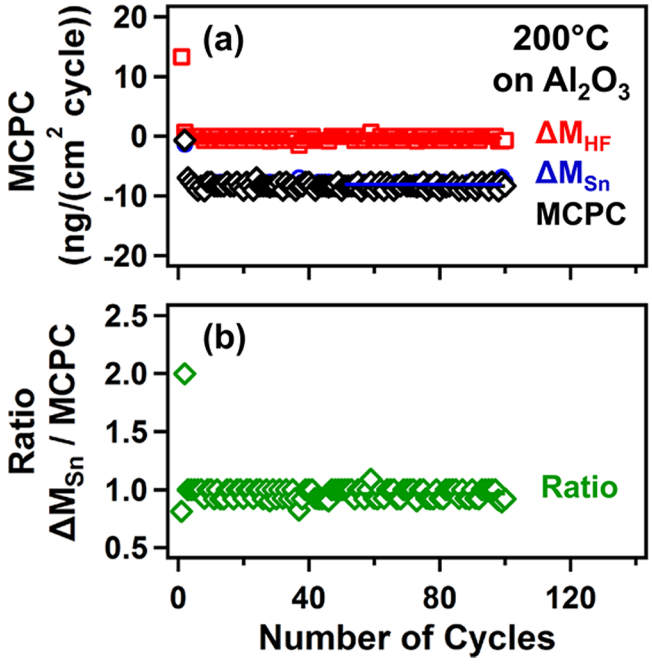

Figure 3. (a) Mass change after the $Sn(acac)_2$ exposure (ΔM_{Sn}), mass change after the HF exposure (ΔM_{HF}), and mass change per cycle (MCPC) versus the number of ALE cycles at 200 °C. (b) ΔM_{Sn}/MCPC ratio versus the number of ALE cycles.

DOI: 10.1021/acs.chemmater.5b00300
Chem. Mater. 2015, 27, 3648−3657

steady-state value of −8.4 ng/(cm^2 cycle) after a nucleation period requiring 3 cycles of Al_2O_3 ALE. Figure 3b displays the ΔM_{Sn}/MCPC ratio during the same 100 cycles. The ΔM_{Sn}/MCPC ratio reaches a steady-state value of 0.97 after a nucleation interval over 3 cycles of Al_2O_3 ALE. The ΔM_{Sn}/MCPC ratio will be used to describe the stoichiometry of the Al_2O_3 ALE reactions.

ΔM_{Sn}, ΔM_{HF}, MCPC, and the ΔM_{Sn}/MCPC ratio at 150−250 °C are summarized in Table 1. All temperatures display a mass loss, and the mass loss is larger at higher temperatures. The mass change after the $Sn(acac)_2$ exposure, ΔM_{Sn}, is mostly responsible for the temperature dependence of the MCPC. An Arrhenius plot is employed to characterize the temperature dependence. Figure 4a shows the Arrhenius plot for the temperature-dependent MCPC. This Arrhenius plot yields an activation barrier of 6.6 ± 0.4 kcal/mol for Al_2O_3 ALE.

Table 1. MCPC, ΔM_{Sn}, ΔM_{HF}, ΔM_{Sn}/MCPC, x, and x(MCPC) for Al_2O_3 ALE at Different Temperatures[a]

temp (°C)	MCPC	ΔM_{Sn}	ΔM_{HF}	ΔM_{Sn}/MCPC	x	x(MCPC)
150	−4.1	0.19	−4.3	−0.067	0.74	−3.0
175	−5.6	−3.2	−2.4	0.57	0.46	−2.6
200	−8.4	−8.1	−0.28	0.97	0.29	−2.4
225	−12.3	−14.6	2.3	1.2	0.19	−2.4
250	−18.3	−24.0	5.7	1.3	0.15	−2.7

[a]MCPC, ΔM_{Sn}, ΔM_{HF}, and x(MCPC) are expressed in units of ng/(cm^2 cycle).

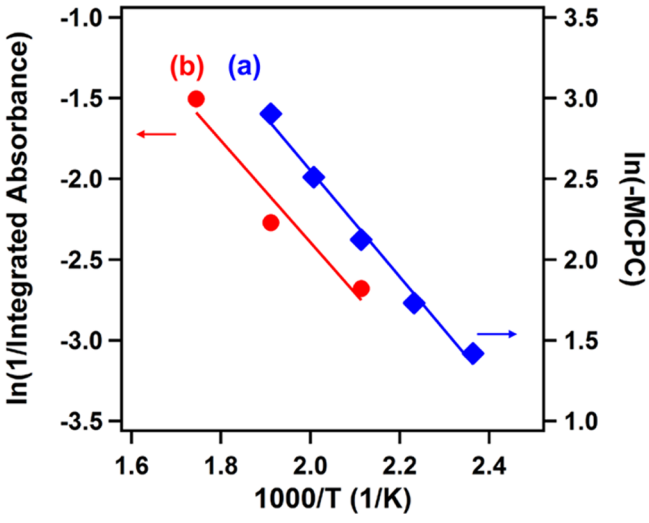

Figure 4. (a) Arrhenius plot of the MCPC. The slope yields an activation barrier of E = 6.6 kcal/mol. (b) Arrhenius plot of 1/(integrated absorbance) for the acetylacetonate vibrational features. The slope yields an activation barrier of E = 6.2 kcal/mol.

B. FTIR Studies of Al_2O_3 ALE. *In situ* FTIR spectra of Al_2O_3 films grown on ZrO_2 nanoparticles using 10 Al_2O_3 ALD cycles at 200 °C are shown in Figure 5. These FTIR spectra are referenced to the initial ZrO_2 nanoparticles. The absorbance feature between 800 and 1000 cm^{-1} is attributed to the Al−O stretching vibrations in bulk Al_2O_3. The absorbance of the Al−O stretching vibrations in amorphous Al_2O_3 is broad and ranges from ~550 to 1030 cm^{-1}.[31,34−36] The breadth of this expected absorbance feature is not observed in Figure 5. The strong absorption from the ZrO_2 nanoparticles at ≤800 cm^{-1} partially obscures the infrared absorbance of the Al−O stretching vibrations. The absorbance feature for the Al−O stretching vibration grows progressively with the Al_2O_3 ALD cycles.

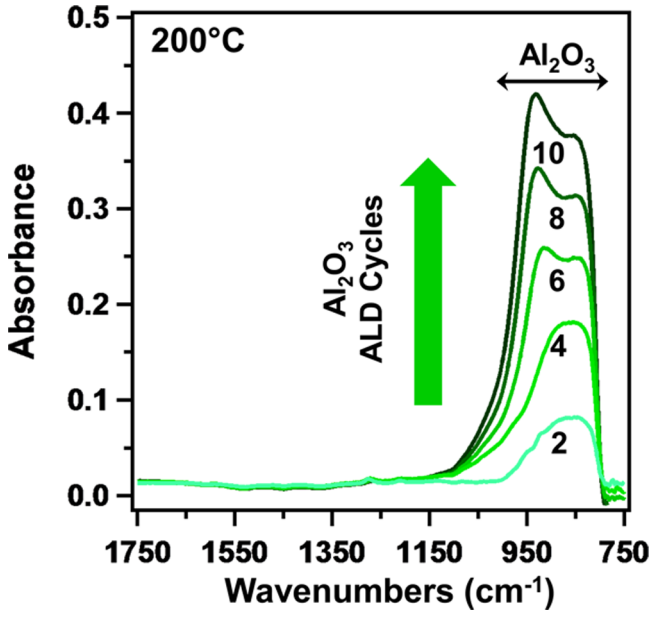

Figure 5. Infrared absorbance showing the growth of Al−O stretching vibrations in bulk Al_2O_3 versus the number of Al_2O_3 ALD cycles at 200 °C. These FTIR spectra were referenced to the initial ZrO_2 nanoparticles.

FTIR spectra during the etching of the Al_2O_3 ALD films on the ZrO_2 nanoparticles at 200 °C are shown in Figure 6. These FTIR spectra were recorded after the $Sn(acac)_2$ exposures and are referenced to the initial ZrO_2 nanoparticles. The absorbance feature from the Al−O stretching vibrations between 800 and 1000 cm^{-1} decreases progressively with Al_2O_3 ALE cycles.

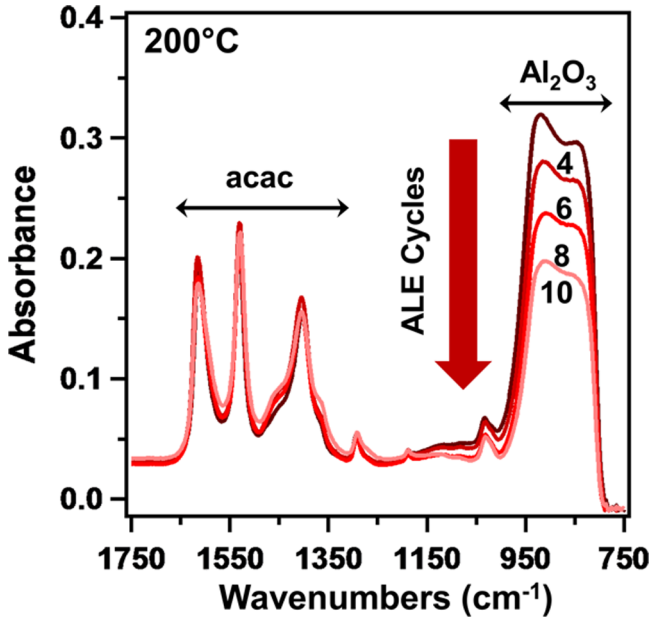

Figure 6. Infrared absorbance showing the loss of Al−O stretching vibrations in bulk Al_2O_3 versus the number of Al_2O_3 ALE cycles at 200 °C. These FTIR spectra were referenced to the initial ZrO_2 nanoparticles.

DOI: 10.1021/acs.chemmater.5b00300
Chem. Mater. 2015, 27, 3648−3657

Infrared absorbance features also appear between 1250 and 1650 cm^{-1} that are attributed to acetylacetonate vibrations from the $Sn(acac)_2$ surface reaction products.[35,36] The absorbance from these acetylacetonate vibrations remains approximately constant after the $Sn(acac)_2$ exposures versus the number of Al_2O_3 ALE cycles.

The FTIR spectra of the absorbance from the acetylacetonate vibrations during Al_2O_3 ALE at 200, 250, and 300 °C are shown after $Sn(acac)_2$ and HF exposures in Figures 7a and 7b,

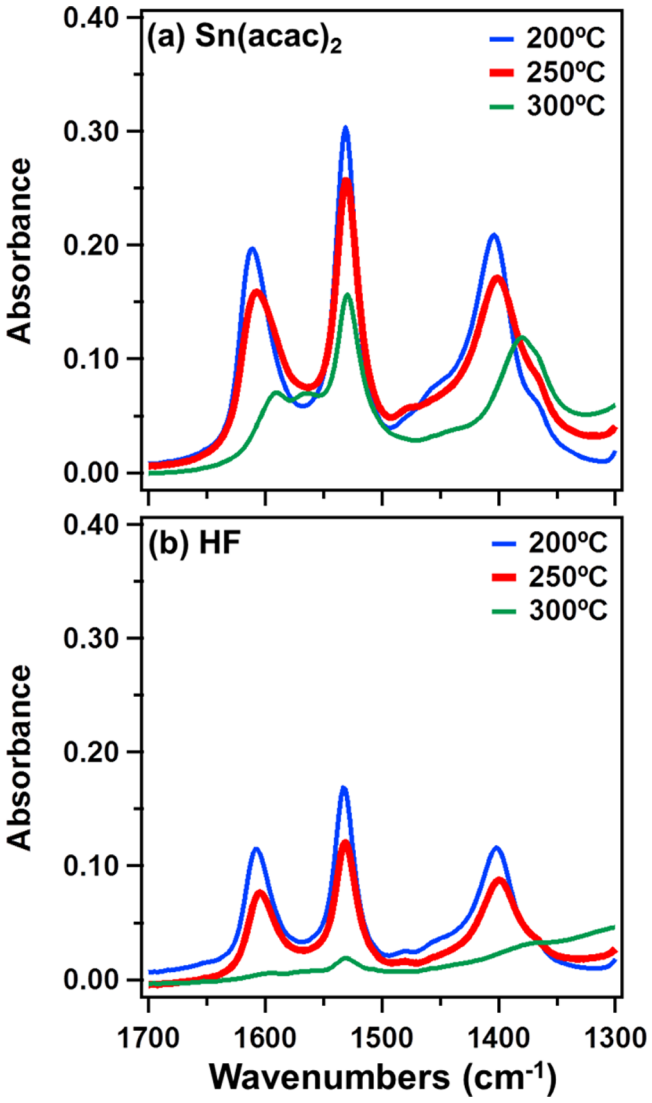

Figure 7. Infrared absorbance from the acetylacetonate vibrations during Al_2O_3 ALE at 200, 250, and 300 °C after (a) $Sn(acac)_2$ exposures and after (b) HF exposures. These FTIR spectra were referenced to the SiO_2 nanoparticles coated with the Al_2O_3 ALD film.

respectively. The absorbance from the acetylacetonate surface species, such as SnF(acac)*, Sn(acac)*, or acac*, decreases at higher temperatures after the $Sn(acac)_2$ exposures in Figure 7a. The astericks are used to indicate surface species. This behavior illustrates that the $Sn(acac)_2$ surface reaction products are more stable at lower surface temperatures.

Figure 7b reveals that the absorbances from the acetylacetonate vibrational features are much lower following the HF exposures. The loss of acetylacetonate vibrational features is expected because HF is believed to react with acetylacetonate species to produce volatile reaction products such as SnF(acac). The absorbance of the remaining acetylacetonate species after HF exposures also decreases dramatically at 300 °C. This behavior indicates that HF exposures are able to remove most of the acetylacetonate species at 300 °C. Based on the peak absorbance for the acetylacetonate vibrational feature at ~1530 cm^{-1}, only ≤10% of the acetylacetonate species remain after HF exposures at 300 °C compared with the acetylacetonate species that remain after HF exposures at 200 °C.

C. Studies of Al_2O_3 ALE Nucleation. QCM and FTIR measurements were employed to study the nucleation of Al_2O_3 ALE during the first $Sn(acac)_2$ and HF exposures. Figure 8

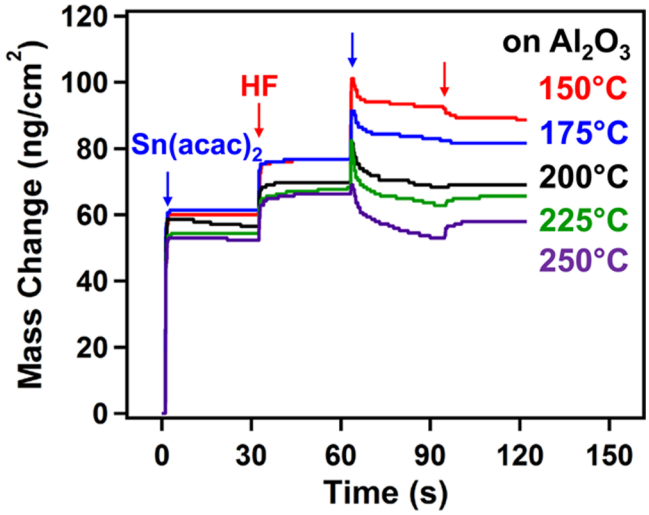

Figure 8. Expansion of first two ALE cycles in Figure 1 showing the individual mass changes during the sequential $Sn(acac)_2$ and HF exposures at 150, 175, 200, 225, and 250 °C.

shows an enlargement of the mass changes during the first two Al_2O_3 ALE cycles for the various temperatures in Figure 1. The first $Sn(acac)_2$ exposure displays mass gains of ΔM_{Sn} = 52−61 ng/cm^2 at 150−250 °C resulting from $Sn(acac)_2$ surface reaction products on the Al_2O_3 film such as Sn(acac)* and acac*. To estimate the coverage of $Sn(acac)_2$* species on the surface, the sites on the Al_2O_3 surface can be approximated using the density of 3.0 g/cm^3 for Al_2O_3 ALD films. This mass density is equivalent to a number density of $\rho = 1.77 \times 10^{22}$ "Al_2O_3 units"/cm^3. This number density yields an estimate for the number of Al_2O_3 units on the Al_2O_3 surface of $\rho^{2/3} = 6.80 \times 10^{14}$ Al_2O_3 units/cm^2 assuming a square lattice. This coverage of Al_2O_3 units represents an Al_2O_3 mass of 115 ng/cm^2.

The coverage of $Sn(acac)_2$* can then be approximated based on the mass gain of 61 ng/cm^2. This mass gain is equivalent to 1.16×10^{14} $Sn(acac)_2/cm^2$. The normalized coverage of $Sn(acac)_2$* relative to Al_2O_3 units on the surface is $(1.16 \times 10^{14}$ $Sn(acac)_2/cm^2)/(6.80 \times 10^{14}$ Al_2O_3 units/$cm^2) = 0.17$ $Sn(acac)_2/(Al_2O_3$ unit). This coverage is reasonable given that $Sn(acac)_2$ may dissociate into Sn(acac)* and acac*. In addition, the acetylacetonate ligand is bulky and expected to occupy more than one Al_2O_3 unit on the Al_2O_3 surface.

The first HF exposure on the Al_2O_3 surface previously exposed to $Sn(acac)_2$ shows mass gains of ΔM_{HF} = 13−17 ng/cm^2 at 150−250 °C. In contrast, the first HF exposure on a fresh Al_2O_3 surface prior to $Sn(acac)_2$ exposures shows mass gains of ΔM_{HF} = 35−38 ng/cm^2 at 150−250 °C. The difference between these mass gains is caused by the amount of $Sn(acac)_2$

DOI: 10.1021/acs.chemmater.5b00300
Chem. Mater. 2015, 27, 3648−3657

reaction products that are removed by the HF exposures and result in a mass loss.

The coverage of HF or HF reaction products can be approximated based on the mass gain of 38 ng/cm^2 following HF exposures on fresh Al_2O_3 surfaces. Assuming that HF is the adsorption product, the mass gain is equivalent to 1.14×10^{15} HF/cm^2. The normalized coverage of HF species relative to Al_2O_3 units on the surface is $(1.14 \times 10^{15}$ HF/cm$^2)/(6.80 \times 10^{14}$ Al_2O_3 units/cm$^2) = 1.68$ HF/(Al_2O_3 unit). This estimated HF coverage is larger than the number of Al_2O_3 units on the Al_2O_3 substrate.

The HF may also react with the Al_2O_3 substrate by the following reaction: $Al_2O_3 + 6HF \rightarrow 2AlF_3 + 3H_2O$. The reaction of HF with γ-Al_2O_3 to produce AlF_3 has been observed at 250 °C.[37] This reaction is predicted to be spontaneous over the temperature range from 150 to 250 °C.[38] The Gibbs free energy changes are negative and decrease slightly in absolute magnitude from $\Delta G = -63.1$ kcal at 150 °C to $\Delta G = -53.8$ kcal at 250 °C.[38]

Assuming that AlF_3 is the reaction product, the mass gain of 38 ng/cm^2 is equivalent to an AlF_3 coverage of 6.93×10^{14} AlF_3/cm^2. The normalized coverage of AlF_3 relative to Al_2O_3 units on the surface is $(6.93 \times 10^{14}$ AlF_3/cm$^2)/(6.80 \times 10^{14}$ Al_2O_3 units/cm$^2) = 1.02$ AlF_3/(Al_2O_3 unit). This estimated AlF_3 coverage is very similar to the number of Al_2O_3 units on the Al_2O_3 substrate.

Subsequent $Sn(acac)_2$ exposures react with the AlF_3 or HF adlayer, and subsequent HF exposures react with the Al_2O_3 substrate and remove $Sn(acac)_2$ adsorption products. At 225 and 250 °C, mass losses begin with the second ALE cycle as shown in Figure 8. At 200 and 175 °C, mass losses begin with the third ALE cycle. At 150 °C, mass losses begin with the fourth ALE cycle.

The nucleation of the Al_2O_3 ALE process was also observed by the FTIR studies. Figure 9 shows the FTIR spectra during the first Al_2O_3 ALE cycle. These FTIR spectra are referenced to the initial ZrO_2 nanoparticles. The infrared absorbance corresponding to the Al−O stretching vibration in bulk Al_2O_3 between 800 and 1000 cm^{-1} decreases slightly with the first $Sn(acac)_2$ exposure. This decrease is attributed to $Sn(acac)_2$ adsorbing on the thin Al_2O_3 film and perturbing the Al−O vibrational modes. Pronounced vibrational features associated with acetylacetonate species on the Al_2O_3 substrate at 1250−1650 cm^{-1} are also observed in Figure 9 after the $Sn(acac)_2$ exposure.[35,36]

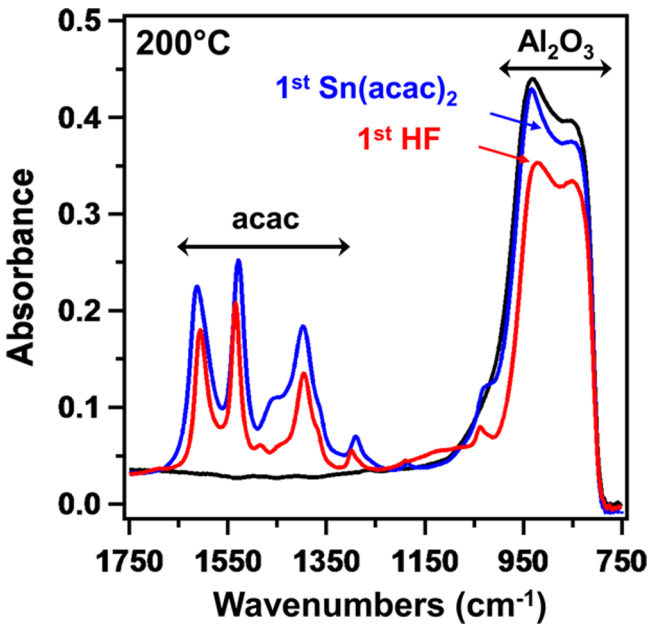

Figure 9. Infrared absorbance showing the Al−O stretching vibrations in bulk Al_2O_3 and the acetylacetonate vibrational features for the first $Sn(acac)_2$ and HF exposures at 200 °C. These FTIR spectra were referenced to the initial ZrO_2 nanoparticles.

Figure 9 also shows that an additional reduction occurs in absorbance features corresponding to the Al−O vibrational modes after the first HF exposure. This reduction is consistent with the conversion of some Al_2O_3 to AlF_3. Figure 9 also shows that the vibrational features of the acetylacetonate species are also decreased after the first HF exposure. This decrease is consistent with HF reacting with the $Sn(acac)_2$ surface reaction products to remove some acetylacetonate species from the Al_2O_3 substrate.

Figure 10 displays the infrared absorbance spectra after the first $Sn(acac)_2$ exposure and first HF exposure on Al_2O_3 films at 200 °C. In contrast to Figures 5, 6, and 9, these FTIR experiments were performed on SiO_2 nanoparticles. Unlike ZrO_2 nanoparticles that absorb infrared radiation between ~400 and 800 cm^{-1}, SiO_2 nanoparticles absorb infrared radiation between 925 and 1400 cm^{-1}, between 700 and 875 cm^{-1}, and between 400 and 650 cm^{-1}. The SiO_2 nanoparticles have an open window at lower frequency to observe the species involved in Al_2O_3 ALD and Al_2O_3 ALE.

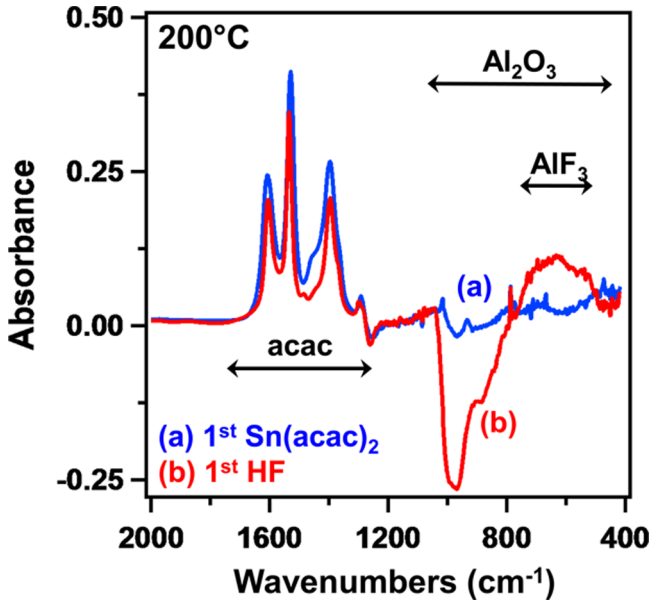

Figure 10. Infrared absorbance after the first $Sn(acac)_2$ exposure and first HF exposure on an Al_2O_3 film at 200 °C. These FTIR spectra were referenced to the SiO_2 nanoparticles coated with the Al_2O_3 ALD film.

The spectra in Figure 10 were referenced to the SiO_2 nanoparticles and the Al_2O_3 ALD film that coated the SiO_2 nanoparticles. The acetylacetonate features were again observed at 1250−1650 cm^{-1}. In addition, an absorbance feature at 500−800 cm^{-1} appeared after the first HF exposure. This feature was assigned to the Al−F stretching vibration in the AlF_3 layer that forms from Al_2O_3 during the HF exposure.[39,40] There was also

DOI: 10.1021/acs.chemmater.5b00300
Chem. Mater. 2015, 27, 3648−3657

an absorbance loss observed at ~1000 cm^{-1} that corresponds with the removal of some absorbance from the Al−O stretching vibration in Al_2O_3 upon AlF_3 formation.

Figure 11 displays the FTIR spectra during Al_2O_3 ALE at 200, 250, and 300 °C. These spectra were again referenced to

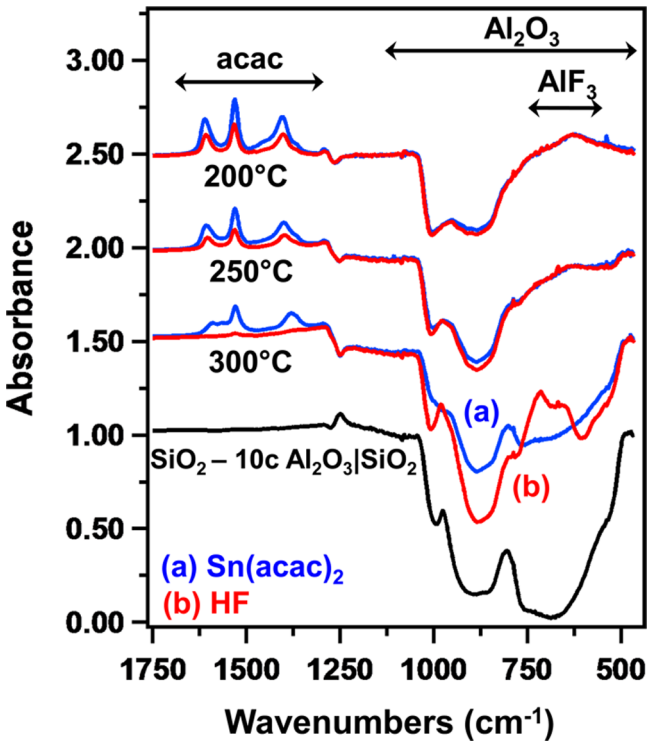

Figure 11. Infrared absorbance during Al_2O_3 ALE at 200, 250, and 300 °C recorded after the $Sn(acac)_2$ exposures and HF exposures. These FTIR spectra were referenced to the SiO_2 nanoparticles coated with the Al_2O_3 ALD film.

the SiO_2 nanoparticles coated with the Al_2O_3 ALD film. Spectra are shown after both the $Sn(acac)_2$ exposures and HF exposures. The absorbance features from acetylacetonate surface species at 1250−1650 cm^{-1} were present after all of the $Sn(acac)_2$ exposures. The acetylacetonate surface species decreased with increasing temperature after both $Sn(acac)_2$ and HF exposures. In addition, most of the acetylacetonate surface species were removed from the surface by the HF exposure at 300 °C.

Figure 11 also reveals that a loss from the absorbance feature assigned to the Al−O stretching vibrations in Al_2O_3 occurs at 200, 250, and 300 °C. This loss appears at 825−1050 cm^{-1} because the absorbance gain from the Al−F stretching vibrations of AlF_3 at 500−800 cm^{-1} partially obscures the loss from the Al−O stretching vibrations in Al_2O_3 at lower frequencies. The spectra after the $Sn(acac)_2$ and HF exposures in the region from 500 to 1050 cm^{-1} were not substantially different at 200 and 250 °C. In contrast, the spectra were distinctly different at 300 °C where the absorbance from the Al−F stretching vibration is nearly completely removed after the $Sn(acac)_2$ exposure and then reappears after the HF exposure. The spectrum at the bottom of Figure 11 is provided for reference and shows the expected absorbance loss corresponding to the removal of 10 cycles of Al_2O_3 ALD.

Figure 12 shows the difference infrared absorbance spectra during Al_2O_3 ALE at 200, 250, and 300 °C. Spectra are

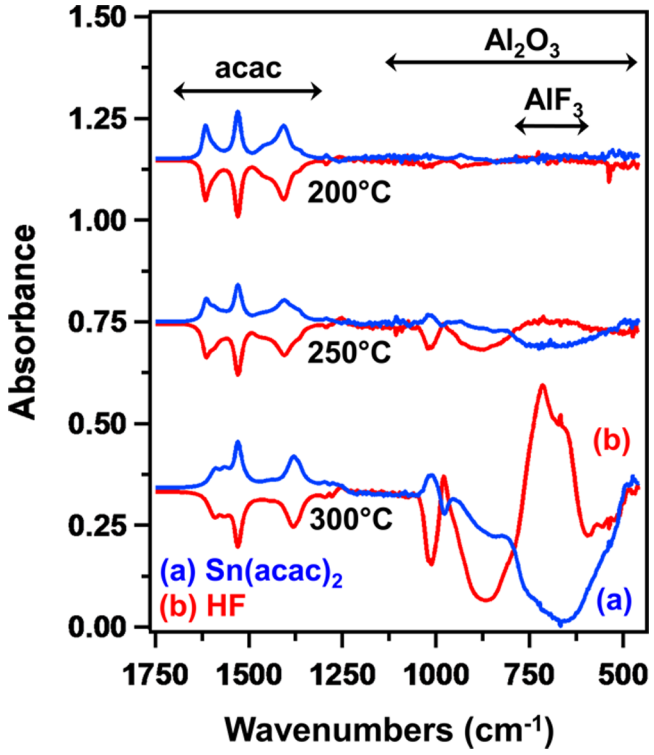

Figure 12. Difference infrared absorbance during Al_2O_3 ALE at 200, 250, and 300 °C. The difference spectra recorded after the $Sn(acac)_2$ and HF exposures were referenced using the spectra after the previous HF and $Sn(acac)_2$ exposures, respectively.

displayed after both the $Sn(acac)_2$ exposures and HF exposures. These difference spectra correspond to the absolute spectra shown in Figure 11. These difference spectra are referenced with respect to the sample after the previous reactant exposure.

The difference spectra in Figure 12 highlight the absorbance changes that occur during the sequential ALE reactions. The absorbance changes for the acetylacetonate surface species are nearly equal and mirror images of each other after the $Sn(acac)_2$ and HF exposures at 200, 250, and 300 °C. In contrast, the absorbance from Al−F vibrations in AlF_3 shows little change at 200 °C and nearly mirror image changes after the $Sn(acac)_2$ and HF exposures at 250 °C. At 300 °C, the absorbance for the Al−F stretching vibrations dramatically appears after the HF exposure and is lost after the $Sn(acac)_2$ exposure.

D. Proposed Al_2O_3 ALE Reaction Mechanism. Figure 13 shows the schematic for the proposed Al_2O_3 ALE surface chemistry. This possible picture for Al_2O_3 ALE is derived from the mass changes during the $Sn(acac)_2$ and HF exposures as determined by the QCM measurements and the vibrational absorbances observed by the FTIR spectroscopy analysis. This scheme does not include species, such as possible acetylacetonate species, that do not change during the $Sn(acac)_2$ and HF exposures. This scheme also assumes that the HF reaction produces AlF_3 on the Al_2O_3 film.

During the $Sn(acac)_2$ reaction shown in Figure 13a, $Sn(acac)_2$ reacts with AlF_3 on the Al_2O_3 substrate. The reaction between $Sn(acac)_2$ and AlF_3 is probably facilitated by Lewis acid−base interactions. The electron lone pair on $Sn(acac)_2$ acts as a Lewis base.[41] AlF_3 is a strong Lewis acid either as a molecule or as a molecular solid.[42−44] The reaction between $Sn(acac)_2$ and AlF_3 is assumed to form volatile SnF(acac) and

DOI: 10.1021/acs.chemmater.5b00300
Chem. Mater. 2015, 27, 3648−3657

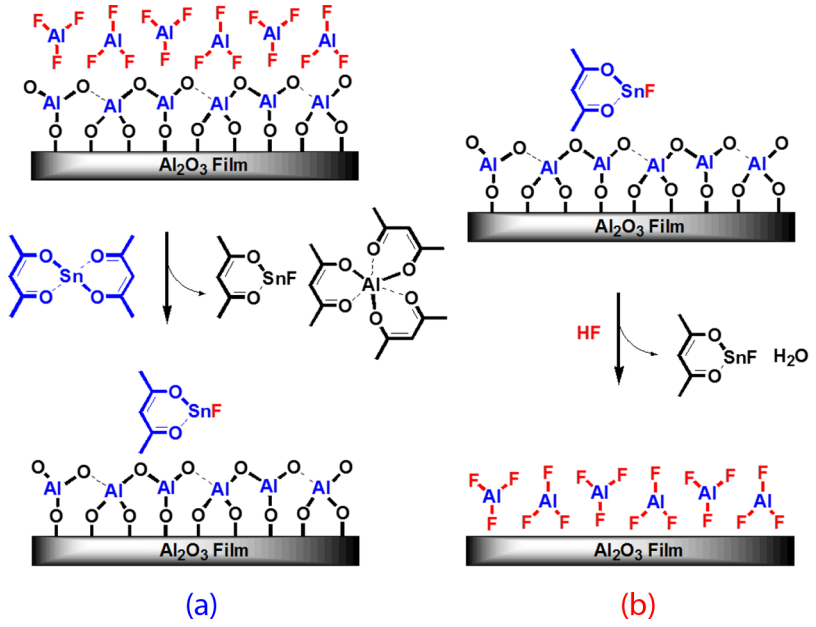

Figure 13. Schematic of proposed surface chemistry for Al_2O_3 ALE showing (a) $Sn(acac)_2$ reaction and (b) HF reaction.

$Al(acac)_3$ reaction products and SnF(acac)* surface species. There is also a possibility that $AlF(acac)_2$ could be a gas phase reaction product. The gas phase reaction products have not yet been identified using mass spectrometry.

AlF_3 has a negligible vapor pressure at the Al_2O_3 ALE temperatures. A measurable vapor pressure for AlF_3 of ~1 × 10^{-3} Torr is obtained only at high temperatures of ~700 °C.[45] $Al(acac)_3$ is a stable metal β-diketonate with a high vapor pressure of ~3−4 Torr at 150 °C.[46−48] The sublimation temperature for $Al(acac)_3$ of ~200 °C has been derived from thermogravimetric studies.[47]

After the AlF_3 layer is lost resulting from $Al(acac)_3$ and SnF(acac) product formation, there may be a strong interaction between the SnF(acac)* surface species and the underlying Al_2O_3 substrate. The electron lone pair on SnF(acac)* can again act as a Lewis base and bind on Lewis acid sites on Al_2O_3. This interaction may lead to SnF(acac)* species adsorbed to the Al_2O_3 substrate.

During the HF reaction shown in Figure 13b, HF reacts with the SnF(acac)* surface species and the underlying Al_2O_3 surface to form AlF_3. In addition, HF also provides hydrogen to form H_2O as a reaction product. This reaction removes the oxygen in Al_2O_3. The AlF_3 layer is then ready for the next $Sn(acac)_2$ reaction.

The overall reaction can be written as

$$Al_2O_3 + 6HF + 6Sn(acac)_2 \rightarrow 2Al(acac)_3 + 6SnF(acac) + 3H_2O \quad (1)$$

This overall reaction can be separated into the $Sn(acac)_2$ and HF reactions:

reaction a of Figure 13:

$$Al_2O_3|2AlF_3^* + 6Sn(acac)_2 \rightarrow Al_2O_3|xSnF(acac)^* + 2Al(acac)_3 + (6-x)SnF(acac) \quad (2)$$

reaction b of Figure 13:

$$Al_2O_3|xSnF(acac)^* + 6HF \rightarrow 2AlF_3^* + xSnF(acac) + 3H_2O \quad (3)$$

These reactions include only species that change during the $Sn(acac)_2$ and HF exposures. There may be other surface species present, such as acetylacetonate species, that do not change during the $Sn(acac)_2$ and HF exposures. The asterisks indicate the surface species and the vertical lines are used to separate the various surface species. AlF_3 is the key reaction intermediate. The production of all of the $Al(acac)_3$ is assumed to occur during reaction a.

The Al_2O_3 shown in eqs 2 and 3 is the amount of Al_2O_3 that is etched during the ALE reactions. Table 1 shows that the amount of Al_2O_3 that is etched during one Al_2O_3 ALE cycle increases with temperature. $2AlF_3$* and SnF(acac)* are also the amounts added during the HF and $Sn(acac)_2$ reactions, respectively. x quantifies SnF(acac)* after the $Sn(acac)_2$ exposures relative to the amount of Al_2O_3 that is etched in one Al_2O_3 ALE cycle.

The parameter x in eqs 2 and 3 is determined by the ΔM_{Sn}, ΔM_{HF} and MCPC values. x can be calculated from the ΔM_{Sn}/MCPC ratio using the following equation:

$$x = (2 \times 84.0 - 102.0(\Delta M_{sn}/\mathrm{MCPC}))/236.8 \quad (4)$$

where 84.0, 102.0, and 236.8 are the molecular weights for AlF_3, Al_2O_3, and SnF(acac), respectively. The temperature dependence of the x values is x = 0.74, 0.46, 0.29, 0.19, and 0.15 at 150, 175, 200, 225, and 250 °C, respectively. These x values are included in Table 1.

The parameter x defines the SnF(acac)* species after the $Sn(acac)_2$ exposures relative to the amount of Al_2O_3 that is etched in one Al_2O_3 ALE cycle. Consequently, the product x(MCPC) provides a measure of the SnF(acac)* species on the surface after the $Sn(acac)_2$ exposures. The x(MCPC) values are included in Table 1. These x(MCPC) values are fairly constant at all of the temperatures. This behavior indicates that the

DOI: 10.1021/acs.chemmater.5b00300
Chem. Mater. 2015, 27, 3648−3657

SnF(acac)* coverage is nearly constant at the different temperatures after the $Sn(acac)_2$ exposures.

The difference infrared absorbance spectra in the acetylacetonate region of the spectra in Figure 12 are consistent with a constant coverage of SnF(acac)* species at the different temperatures after the $Sn(acac)_2$ exposures. Figure 12 shows that the changes in the absorbance in the acetylacetonate region after $Sn(acac)_2$ and HF exposures are very similar at 200, 250, and 300 °C. This constant absorbance change can be identified with the SnF(acac)* surface species that are added and then removed during the $Sn(acac)_2$ and HF exposures, respectively, as described by eqs 2 and 3.

The SnF(acac)* coverage after the $Sn(acac)_2$ exposures can be determined from the amount of Al_2O_3 that is etched in one Al_2O_3 ALE cycle. For example, the MCPC of −5.6 ng/cm^2 at 175 °C represents a coverage of 3.3×10^{13} Al_2O_3 units/cm^2. This conversion is based on 1.69×10^{-22} g/(Al_2O_3 unit). This coverage of Al_2O_3 units multiplied by the x value of 0.46 at 175 °C yields a SnF(acac)* coverage of 1.52×10^{13} SnF(acac)*/cm^2. The MCPC and x values at the other temperatures also yield similar SnF(acac)* coverages that vary from 1.38 to 1.77 $\times 10^{13}$ SnF(acac)*/cm^2.

The nearly constant SnF(acac)* coverage of $\sim 1.5 \times 10^{13}$ SnF(acac)*/cm^2 can be compared with the number of Al_2O_3 units on the Al_2O_3 surface of 6.80×10^{14} Al_2O_3 units/cm^2. The normalized coverage of SnF(acac)* relative to Al_2O_3 units on the surface is ($\sim 1.5 \times 10^{13}$ SnF(acac)*/cm^2)/(6.80×10^{14} Al_2O_3 units/cm^2) = ∼0.022 SnF(acac)*/(Al_2O_3 unit). This normalized coverage is ∼2.2% of an Al_2O_3 unit monolayer. This coverage may represent a saturated layer of SnF(acac)* species on the Al_2O_3 surface. The normalized coverage of ∼2.2% is somewhat low. However, perhaps the SnF(acac)* species bind only on particular Lewis acid sites on the Al_2O_3 surface.

Although the absolute SnF(acac)* coverage derived from the QCM measurements after the $Sn(acac)_2$ exposures is very similar at the different temperatures, the FTIR experiments reveal that the total coverage of acetylacetonate species has a large change with temperature as shown in Figure 7. Figure 4b shows the effective Arrhenius dependence of 1/(integrated absorbance) for the acetylacetonate vibrational features at 200, 250, and 300 °C in Figure 7b after the HF exposures. This effective Arrhenius plot yields an activation barrier of $E = 6.2 \pm 1.5$ kcal/mol. This activation barrier is very similar to the activation barrier of $E = 6.6 \pm 0.4$ kcal/mol derived from the temperature-dependent MCPC values in Figure 4. Nearly identical results were obtained from the effective Arrhenius analysis of the temperature-dependent coverage of acetylacetonate species after the $Sn(acac)_2$ exposure.

The correlation between the two Arrhenius plots in Figure 4 suggests that the MCPC is inversely dependent on the coverage of acetylacetonate species remaining on the surface after the HF or $Sn(acac)_2$ exposures. Higher coverages of acetylacetonate species are correlated with lower Al_2O_3 ALE rates. An inverse dependence between MCPC and the coverage of acetylacetonate species would be expected if there is a site-blocking effect of acetylacetonate species on Al_2O_3 ALE. Similar site-blocking effects of acetylacetonate species were observed for Pt ALD and Pd ALD.[49,50] The acetylacetonate species could either restrict the fluorination of Al_2O_3 to produce AlF_3 during the HF exposure or the ligand exchange between $Sn(acac)_2$ and AlF_3 during the $Sn(acac)_2$ exposure. The dramatic increase in AlF_3 species produced at 300 °C after the HF exposure in Figure 12 argues that the primary site-blocking effect of the acetylacetonate species may be on the fluorination reaction.

The proposed reactions for Al_2O_3 ALE are very similar to the reactions proposed earlier for HfO_2 ALE.[26] Both Al_2O_3 ALE and HfO_2 ALE display etching rates that increase at higher temperatures. These temperature-dependent etching rates are both believed to be correlated inversely with the acetylacetonate coverage on the substrate after the HF or $Sn(acac)_2$ exposures. The $Al(acac)_3$ and $Hf(acac)_4$ etching products are both volatile. Both Al_2O_3 and HfO_2 form stable fluorides upon exposure to HF. The etching rates for Al_2O_3 ALE are somewhat higher than the etching rates for HfO_2 ALE. These differences may be related to the more favorable thermochemistry for Al_2O_3 ALE. The ΔG for the HF reaction with HfO_2 is not as favorable as the ΔG for the HF reaction with Al_2O_3.[38]

IV. CONCLUSIONS

In situ quartz crystal microbalance (QCM) and Fourier transform infrared (FTIR) spectroscopy measurements were used to explore the mechanism of thermal Al_2O_3 atomic layer etching (ALE) using $Sn(acac)_2$ and HF as the reactants. The mass change per cycle (MCPC) for Al_2O_3 ALE varied with temperature from −4.1 ng/(cm^2 cycle) at 150 °C to −18.3 ng/(cm^2 cycle) at 250 °C. These temperature-dependent etch rates yielded an activation barrier for Al_2O_3 ALE of $E = 6.6 \pm 0.4$ kcal/mol. The mass changes after the $Sn(acac)_2$ and HF exposures were also dependent on temperature. The mass changes after the $Sn(acac)_2$ exposures indicated that more $Sn(acac)_2$ surface reaction products were present at lower temperatures. The mass changes after the HF exposures indicated that more AlF_3 species were present at higher temperatures.

FTIR spectroscopy measurements monitored the Al_2O_3 ALE and quantified the acetylacetonate surface species versus temperature. A connection was observed between the MCPC values and the absorbance from the acetylacetonate species. The Al_2O_3 ALE rate was inversely dependent on the acetylacetonate surface species. This behavior suggested that the acetylacetonate surface species may have a site-blocking effect on Al_2O_3 ALE. Difference infrared absorbance spectra also revealed that there was a constant absorbance change in the acetylacetonate spectral region at all temperatures. This constant absorbance change may be attributed to the constant coverage of SnF(acac)* species after the $Sn(acac)_2$ exposures at all temperatures determined by the QCM analysis.

The nucleation of the Al_2O_3 ALE was also explored using QCM and FTIR measurements. The conversion of Al_2O_3 to AlF_3 was consistent with a large mass gain and loss of infrared absorbance of Al−O stretching vibrations after the initial HF exposure on the Al_2O_3 film. The formation of AlF_3 after the initial HF exposure and the presence of AlF_3 on the surface after each HF exposure during Al_2O_3 ALE were also observed by FTIR experiments. These results suggest that AlF_3 is the key reaction intermediate during Al_2O_3 ALE. The HF exposure converts Al_2O_3 to AlF_3, and then the AlF_3 is removed by the $Sn(acac)_2$ exposure.

■ AUTHOR INFORMATION

Corresponding Author

*E-mail: steven.george@colorado.edu.

Notes

The authors declare no competing financial interest.

DOI: 10.1021/acs.chemmater.5b00300
Chem. Mater. 2015, 27, 3648−3657

■ ACKNOWLEDGMENTS

This research was funded by the National Science Foundation (Grant CHE-1306131). Additional personnel support for Y.L. was provided by the Department of Energy through the DOE-BATT program.

■ REFERENCES

(1) Agarwal, A.; Kushner, M. J. *J. Vac. Sci. Technol., A* **2009**, *27*, 37−50.
(2) Athavale, S. D.; Economou, D. J. *J. Vac. Sci. Technol., A* **1995**, *13*, 966−971.
(3) Athavale, S. D.; Economou, D. J. *J. Vac. Sci. Technol., B: Micorelectron. Nanometer Struct.—Process., Meas., Phenom.* **1996**, *14*, 3702−3705.
(4) George, S. M. *Chem. Rev.* **2010**, *110*, 111−131.
(5) Leskela, M.; Ritala, M. *Angew. Chem., Int. Ed.* **2003**, *42*, 5548−5554.
(6) Marchack, N.; Chang, J. P. *J. Phys. D: Appl. Phys.* **2011**, *44*, No. 174011.
(7) Kubota, N. A.; Economou, D. J.; Plimpton, S. J. *J. Appl. Phys.* **1998**, *83*, 4055−4063.
(8) Park, S. D.; Lee, D. H.; Yeom, G. Y. *Electrochem. Solid-State Lett.* **2005**, *8*, C106−C109.
(9) Park, S. D.; Lim, W. S.; Park, B. J.; Lee, H. C.; Bae, J. W.; Yeom, G. Y. *Electrochem. Solid-State Lett.* **2008**, *11*, H71−H73.
(10) Sakaue, H.; Iseda, S.; Asami, K.; Yamamoto, J.; Hirose, M.; Horiike, Y. *Jpn. J. Appl. Phys. 1* **1990**, *29*, 2648−2652.
(11) Yamamoto, J.; Kawasaki, T.; Sakaue, H.; Shingubara, S.; Horiike, Y. *Thin Solid Films* **1993**, *225*, 124−129.
(12) Sugiyama, T.; Matsuura, T.; Murota, J. *Appl. Surf. Sci.* **1997**, *112*, 187−190.
(13) Lim, W. S.; Park, S. D.; Park, B. J.; Yeom, G. Y. *Surf. Coat. Technol.* **2008**, *202*, 5701−5704.
(14) Meguro, T.; Hamagaki, M.; Modaressi, S.; Hara, T.; Aoyagi, Y.; Ishii, M.; Yamamoto, Y. *Appl. Phys. Lett.* **1990**, *56*, 1552−1554.
(15) Meguro, T.; Ishii, M.; Sugano, T.; Gamo, K.; Aoyagi, Y. *Appl. Surf. Sci.* **1994**, *82*−*83*, 193−199.
(16) Park, S. D.; Oh, C. K.; Bae, J. W.; Yeom, G. Y.; Kim, T. W.; Song, J. I.; Jang, J. H. *Appl. Phys. Lett.* **2006**, *89*, No. 043109.
(17) Lim, W. S.; Park, J. B.; Park, J. Y.; Park, B. J.; Yeom, G. Y. *J. Nanosci. Nanotechnol.* **2009**, *9*, 7379−7382.
(18) Metzler, D.; Bruce, R. L.; Engelmann, S.; Joseph, E. A.; Oehrlein, G. S. *J. Vac. Sci. Technol., A* **2014**, *32*, No. 020603.
(19) Min, K. S.; Kang, S. H.; Kim, J. K.; Jhon, Y. I.; Jhon, M. S.; Yeom, G. Y. *Microelectron. Eng.* **2013**, *110*, 457−460.
(20) Park, J. B.; Lim, W. S.; Park, B. J.; Park, I. H.; Kim, Y. W.; Yeom, G. Y. *J. Phys. D: Appl. Phys.* **2009**, *42*, No. 055202.
(21) Park, J. B.; Lim, W. S.; Park, S. D.; Park, Y. J.; Yeom, G. Y. *J. Korean Phys. Soc.* **2009**, *54*, 976−980.
(22) Kim, Y. Y.; Lim, W. S.; Park, J. B.; Yeom, G. Y. *J. Electrochem. Soc.* **2011**, *158*, D710−D714.
(23) Lim, W. S.; Kim, Y. Y.; Kim, H.; Jang, S.; Kwon, N.; Park, B. J.; Ahn, J.-H.; Chung, I.; Hong, B. H.; Yeom, G. Y. *Carbon* **2012**, *50*, 429−435.
(24) Vogli, E.; Metzler, D.; Oehrlein, G. S. *Appl. Phys. Lett.* **2013**, *102*, No. 253105.
(25) Lee, Y.; George, S. M. *ACS Nano* **2015**, *9*, 2061−2070.
(26) Lee, Y.; DuMont, J. W.; George, S. M. *ECS J. Solid State Sci. Technol.* **2015**, *4*, N5013−N5022.
(27) Elam, J. W.; Groner, M. D.; George, S. M. *Rev. Sci. Instrum.* **2002**, *73*, 2981−2987.
(28) Riha, S. C.; Libera, J. A.; Elam, J. W.; Martinson, A. B. F. *Rev. Sci. Instrum.* **2012**, *83*, No. 094101.
(29) Olah, G. A.; Nojima, M.; Kerekes, I. *Synthesis* **1973**, *12*, 779−780.
(30) DuMont, J. W.; George, S. M. *J. Phys. Chem. C* **2015**, in press (DOI:10.1021/jp512074n).
(31) Ferguson, J. D.; Weimer, A. W.; George, S. M. *Thin Solid Films* **2000**, *371*, 95−104.
(32) Ballinger, T. H.; Wong, J. C. S.; Yates, J. T. *Langmuir* **1992**, *8*, 1676−1678.
(33) Sneh, O.; George, S. M. *J. Phys. Chem.* **1995**, *99*, 4639−4647.
(34) Sindorf, D. W.; Maciel, G. E. *J. Am. Chem. Soc.* **1983**, *105*, 1487−1493.
(35) Nakamoto, K.; Martell, A. E.; McCarthy, P. J. *J. Am. Chem. Soc.* **1961**, *83*, 1272−1276.
(36) Tayyari, S. F.; Milani-nejad, F. *Spectrochim. Acta, Part A* **2000**, *56*, 2679−2691.
(37) Jia, W.-Z.; Lu, J.-Q.; Chen, P.; Wang, Y.-J.; Luo, M.-F. *J. Mater. Chem.* **2011**, *21*, 8987−8990.
(38) *HSC Chemistry*, version 5.1; Outokumpu Research Oy: Pori, Finland.
(39) Koenig, R.; Scholz, G.; Scheurell, K.; Heidemann, D.; Buchem, I.; Unger, W. E. S.; Kemnitz, E. *J. Fluorine Chem.* **2010**, *131*, 91−97.
(40) Gross, U.; Ruediger, S.; Kemnitz, E.; Brzezinka, K.-W.; Mukhopadhyay, S.; Bailey, C.; Wander, A.; Harrison, N. *J. Phys. Chem. A* **2007**, *111*, 5813−5819.
(41) Ewings, P. F. R.; Harrison, P. G.; Fenton, D. E. *J. Chem. Soc., Dalton Trans. (1972-1999)* **1975**, 821−826.
(42) Ball, D. W. *J. Phys. Chem.* **1995**, *99*, 12786−12789.
(43) Krahl, T.; Vimont, A.; Eltanany, G.; Daturi, M.; Kemnitz, E. *J. Phys. Chem. C* **2007**, *111*, 18317−18325.
(44) Wander, A.; Bailey, C. L.; Searle, B. G.; Mukhopadhyay, S.; Harrison, N. M. *Phys. Chem. Chem. Phys.* **2005**, *7*, 3989−3993.
(45) Brunetti, B.; Piacente, V.; Scardala, P. *J. Chem. Eng. Data* **2009**, *54*, 940−944.
(46) Berg, E. W.; Truemper, J. T. *Anal. Chim. Acta* **1965**, *32*, 245−252.
(47) Eisentraut, K. J.; Sievers, R. E. *J. Inorg. Nucl. Chem.* **1967**, *29*, 1931−1936.
(48) Fahlman, B. D.; Barron, A. R. *Adv. Mater. Opt. Electron.* **2000**, *10*, 223−232.
(49) Anderson, V. R.; Leick, N.; Clancey, J. W.; Hurst, K. E.; Jones, K. M.; Dillon, A. C.; George, S. M. *J. Phys. Chem. C* **2014**, *118*, 8960−8970.
(50) Goldstein, D. N.; George, S. M. *Thin Solid Films* **2011**, *519*, 5339−5347.

DOI: 10.1021/acs.chemmater.5b00300
Chem. Mater. 2015, 27, 3648−3657